Date 2011
Author O.A.J. Peters and R.H.M. Huijsmans

Address Delft University of Technology
Ship Hydromechanics Laboratory
Mekelweg 2, 2628 CD Delft

TUDelft

Delft University of Technology

Assessing hydrodynamic behavior during offshore loading and discharge in the heavy marine transport

by

O.A.J. Peters and Rene Huijsmans

Report No. 1805-P **2011**

Published in: Proceedings of the ASME 2011 30th International Conference on Ocean, Offshore and Arctic Engineering, OMAE2011, 19- 24 June 2011, Rotterdam, The Netherlands

OMAE 2011 Rotterdam, NL

30th International Conference on Ocean, Offshore and Arctic Engineering
Rotterdam, The Netherlands June 19 - 24, 2011

Technical Symposia

- **Offshore Technology**
- **Structures, Safety and Reliability**
- **Materials Technology**
- **Pipeline and Riser Technology**
- **Ocean Space Utilization**
- **Ocean Engineering**
- **Polar and Arctic Sciences and Technology**
- **CFD and VIV**
- **Ocean Renewable Energy**
- **Offshore Geotechnics**
- **Jan Vugts Symposium on 'Design Methodology of Offshore Structures'**
- **Jo Pinkster Symposium on 'Second Order Wave Drift Forces on Floating Structures'**
- **Johan Wichers Symposium on 'Mooring of Floating Structures in Waves'**

Welcome to the OMAE2011 DVD.

This DVD contains the final papers of the ASME 2011 30th International Conference on Ocean, Offshore and Arctic Engineering. To locate papers, you can do one of the following:

1. Search. You can perform a fielded search of the title, author(s) name, affiliation or paper number.
2. Review the papers listed in the symposia.
3. Browse the Author Index.

This DVD is best viewed with a Java 1.4.2 (or higher) enabled web browser.

You will need Acrobat Reader 7.0 or higher to view the PDF files.

ASME

ASME NO-SHOW POLICY

According to ASME's no-show policy, if a paper is not presented at the Conference, the paper will not be

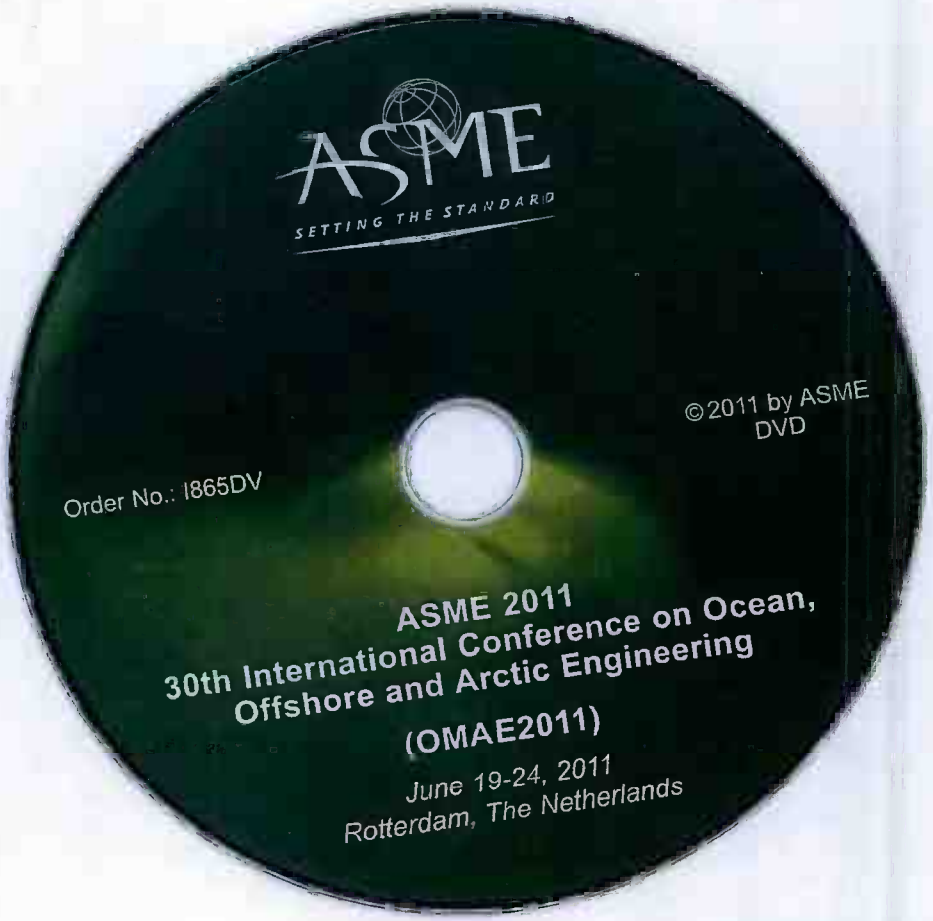
ASME
SETTING THE STANDARD
Order No.: I865DV
©2011 by ASME
DVD
ASME 2011
30th International Conference on Ocean,
Offshore and Arctic Engineering
(OMAE2011)
June 19-24, 2011
Rotterdam, The Netherlands

Proceedings of the ASME 2011 30th International Conference on Ocean, Offshore and Arctic Engineering
OMAE2011
June 19-24, 2011, Rotterdam, The Netherlands

OMAE2011-49174

ASSESSING HYDRODYNAMIC BEHAVIOR DURING OFFSHORE LOADING AND DISCHARGE IN THE HEAVY MARINE TRANSPORT

O.A.J. Peters, MSc*
Dockwise Shipping B.V.
P.O.Box 3208, 4800 DE, Breda
Netherlands

Prof. Dr. Ir. R.H.M. Huijsmans
Delft University of Technology
Mekelweg 2, 2628 CD, Delft
Netherlands

ABSTRACT

Heavy Marine Transport is a well accepted method to move large heavy offshore related floating structures around the world. This type of transport is normally limited to getting from and going to sheltered locations, where loading and discharge operation of these objects are safely carried out in very mild environment. However, there is an increasing demand for loading and discharge at offshore locations; and as these operations are sensitive to environmental criteria, this has consequences for the scheduling issues. Also, with increasing size and weight of offshore structures and the desire to deliver these objects directly to remote offshore location, larger Heavy Transport Vessels are required, which may need to operate in higher sea-states than presently considered safe. These safe conditions are mainly based on long term experience. Assessment of the hydrodynamic behavior of submerged HTVs and cargo in rough seaway, in short Offshore Loading / Discharge, will contribute to extending the scope and operability of HTVs. Also, this investigation will contribute to safety by creating more insight in heavy transport operations.

Research and development projects in the past have dealt with many aspects of Offshore Loading/Discharge. Both the basic design (of both HTV and systems) and hydrodynamic behavior are investigated. Problems were encountered in the area of predicting the relative behavior of floating structure above a HTV. Investigations have shown that inaccuracy is mainly caused due to the narrow gap between cargo and HTV.

Development of an accurate, quick and cost-effective method for the prediction of hydrodynamic behavior of cargo floating above a HTV is in progress. This paper is presenting theory and limitations of an adapted multi-body diffraction theory. The adapted theory uses different domains in which different solution methods are used. For the flow in the gap between cargo and HTV, a 2D solution is used, whereas for the outside domain standard 3D potential solution is applied.

Because of analogy with the single-body floating object in shallow water with narrow gap between body and seafloor, model tests have been performed with different shapes; these shapes are representing typical cargos. The results of the measurements for the different shapes are compared and gap flow phenomenon is explained.

INTRODUCTION

Despite of a few accidents or damages in the past, loading and discharge operations in the Heavy Marine Transport sector is considered very safe; never were they related to excessive motions in waves. This is mainly because these operations take place in sheltered locations during extremely benign conditions, i.e. low wind speeds and virtually no waves. In the rare occasion that operations had to be carried out in areas open to the elements – near shore operations – exposure to weather gave a higher risk of downtime. Then, "Go-No-Go" of the operations is decided by the Master, the Superintendent and the Marine Warranty Surveyor, normally based on general guidelines set at beforehand, weather forecasts and visual estimate of HTV and cargo behavior. The general guidelines are based on long term experience; not on extended analyses and/or model testing.

Driven by desires of designers and yards and the expectation of growing size and weight of potential cargo, recent plans have lead to build a one-of-a-kind super HTV, see Annex A - Figure 10. Because of its size less sheltered locations are available to carry out loading and discharge operations. Also, by extending the scope to offshore operations the super HTV can economize development of remote offshore locations as she can deliver fully commissioned platforms at the desired location. But of course, all other types of HTVs – as shown in Annex A – can be made available for offshore loading and discharge operations.

* PhD student at Delft University of Technology

Therefore, research is needed to make offshore loading and discharge possible outside the standard operational profile. This is required to safeguard operations without accidents and/or damages; also it gives more insight in the state-of-the-art operations.

In other words, to support the ambition to go beyond the standard operational profile, one cannot ignore the effort to investigate the behavior of HTV and cargo during loading and discharge operations. Such an investigation comprises of identifying the hydrodynamic issues and phenomenon, model testing, studying available calculation methods, adapting existing and creating new methods.

RELEVANT SHIP TYPES AND CARGOS

A list of existing and future HTVs is given in Table 1 of Annex A. Four types of semi-submersible heavy transport vessels can be identified:

type 0. Open stern + bow – distinguished by a flat deck from stern to bow; accommodation casing is placed at one side of the vessel, several casings are used at flexible locations, see Figure 10.

type 1. Open stern – these are characterized by large forecastle with accommodation and an open deck to the stern. For longitudinal stability during submergence casings are placed at the stern; sometimes these casings are fixed to accommodate the engine room exhaust system, but mostly they can be freely located anywhere on deck, see Figure 11.

type 2. Closed stern – these ships are mostly converted conventional ships with a lowered section amidships, see Figure 12.

type 3. Dock-type – these are ships with dock walls on each side of the deck and a ramp/door at the stern, see Figure 13.

Numerous types of floating cargos are transported all over the world; e.g. dredging equipment, navy vessels, jack-ups, semi-submersibles, tension leg platforms and FPSOs. Generally these cargos can be represented by a few basic shapes:

- rectangular box shapes, e.g. FPSOs, barges, etc.;
- triangular box shapes, e.g. three-legged jack-ups;
- ring-floaters, e.g. TLPs and Semi submersibles;
- cylindrical shapes; e.g. FPSOs

HYDRODYNAMIC ISSUES

Each HTV type has its own problems concerning prediction of motion characteristics when submerged.

For all types, the submerged deck (Figure 1) can be identified as a local shallow water problem, where the transition between deck and "deep" water domain gives difficulties in solving the diffraction problem. For type 1 the forecastle and type-2 also the castle at the stern have a large influence on the diffraction solution for the deck area; standing waves characterized by the deck length between stern- and forecastle. In addition all HTV types have a relative small water plane area at submerged draft relative to normal sailing draft; this is especially the case for the type 0. With very small water plane area and large mass, the natural frequencies for heave, roll and pitch become very low; this can result in large response due to second order excitation. The aspects mentioned in this paragraph are - to some extend - relevant to semi-submersible drilling rigs, production platforms and heavy derrick crane vessels. These types of vessels are also characterized by a submerged deck of the pontoons and a small water plane area.

For the type 3 HTV the enclosed area – dock – is hardly influenced by waves, however waves are generated inside the dock due to the vertical moving open stern. This problem is similar to Landing Platform Dock ships, as investigated by Straten [1] and Bass [2].

One more specific hydrodynamic issue during loading and discharge of cargo from a HTV is that a very small gap exists between cargo and HTV deck. The influence of such a gap is known as cushioning effect. Jonge [3] studied this gap problem based on work done by Drobyshevski [4].

Many studies, model test and experience from practice have shown that the standard multi-body diffraction – commercially available – is not able to accurately capture the above mentioned problems.

Figure 1: Submerged deck

MULTI DOMAIN DIFFRACTION METHOD

To capture the hydrodynamic issues and improve the accuracy of results, the multi domain method can be applied. This method was clearly described by Pinkster [5], where it is used for passing ships in ports – channels and harbor docks with different water depth were defined as separate domains. At the boundary between each domain, the momentum flux must be continuous.

A short outline of the theory applicable for offshore loading/discharge involving multi-bodies with multi-domains as can be identified based on the previous section. First, the basic multi-body diffraction theory is given. Second, additional methods and/or boundary conditions for the multi-domain are described.

Basic Multi-body Theory

The 3D diffraction theory is based on using the gradient of a scalar potential (Φ) to describe the velocity of the fluid around a number of bodies within a control volume. When this scalar at any location is known, the pressure at that location is known; subsequently, with pressure known on each body, forces are known and finally motions can be determined. For completeness, the well-known basic assumptions and principles are given here:

- The fluid is assumed to be inviscid, homogeneous, incompressible and irrotational
- The method is restricted to bodies with zero mean forward speed
- The amplitudes of waves and motions are assumed to be small compared to the wave length
- The surface of a body is defined by its mean wetted surface
- In regular waves a linear potential, which is a function of the earth fixed co-ordinates *(x, y, z)* and of time *t*, can be written as a product of a co-ordinate dependent part and a harmonic time dependent part as follows:

$$\Phi(x,y,z,t) = \phi(x,y,z)e^{-i\omega t} \qquad \text{(Eq. 1)}$$

- Within the hydrodynamic diffraction theory the potential in an arbitrary point is built up of the following components:
  Φ_w = Potential due to the undisturbed incident wave
  Φ_d = Potential due to diffraction of the undisturbed wave on all fixed bodies
  Φ_R = Potential due to radiated waves by the moving bodies

$$\Phi(x,y,z,t) = \Phi_w + \Phi_d + \Phi_R \qquad \text{(Eq. 2)}$$

with:

$$\Phi_R = \sum_{ib=1}^{N_B}\sum_{j=1}^{6}\Phi_{ib,j} \qquad \text{(Eq. 3)}$$

$\Phi_{ib,j}$ = Potential due to the *j*-mode of motion of body *ib*
N_B = Number of bodies

The potential Φ_w is an input parameter of the calculation, and is defined by the wave frequency, wave height and earth fixed co-ordinate. The potentials Φ_d and Φ_R are dependent of the undisturbed wave and the body shapes; as these potentials are unknown, these will have to be solved to get the forces and motions of the bodies. In following equations Φ_w is represented by Φ_0 and Φ_d is represented by Φ_7.

The control volume is described by the bodies, the free-water surface, the sea-bottom and a cylindrical surface at great distance of the bodies. In the fluid domain of the control volume the potentials have to satisfy the equation of continuity or Laplace equations:

$$\frac{\partial^2\Phi}{\partial x^2} + \frac{\partial^2\Phi}{\partial y^2} + \frac{\partial^2\Phi}{\partial z^2} = 0 \qquad \text{(Eq. 4)}$$

At the boundary of the control volume, the boundary conditions have to be satisfied, which are:

- at free-water surface, pressure is constant and fluid particles cannot pass the boundary,

$$g\frac{\partial\Phi}{\partial z} + \frac{\partial^2\Phi}{\partial t^2} = 0 \qquad \text{for } z = 0 \qquad \text{(Eq. 5)}$$

- fluid cannot pass the sea-bottom

$$\frac{\partial\Phi}{\partial z} = 0 \qquad \text{for } z = -h \qquad \text{(Eq. 6)}$$

  where *h* is the global water depth.
- fluid cannot pass the bodies

$$\frac{\partial\Phi}{\partial n} = \vec{v}_{ib}.\vec{n}_{ib} \qquad \text{on } S_{ib} \text{ for } ib = 1, N_B \qquad \text{(Eq. 7)}$$

- at the cylindrical surface at great distance the bodies the body motions and diffraction potentials need to satisfy the radiation condition, i.e. at great distance Φ_d and $\Phi_{ib,j}$ go to zero.

The velocity potentials of the diffracted wave and the six modes of motion can be represented by a continuous distribution of sources on the surface of the bodies (S_{ib}):

$$\phi_{ib,j}(x,y,z) = \sum_{jb=1}^{N_B}\frac{1}{4\pi}\iint_{S_{jb}}\sigma_{ib,j}(\vec{A}_{jb})G(\vec{X},\vec{A}_{jb})dS_{jb} \qquad \text{(Eq. 8)}$$

with:

$\vec{X} = (x,y,z)$, i.e. position vector of field point on body *ib*

$\vec{A}_{jb} = (A_1, A_2, A_3)$, i.e. position vector of source on body *jb*

j =1,7

ib =1,N_B

In (Eq. 8), $\sigma_{jb,j}$ is the source strength at a point with earth fixed co-ordinates (A_1,A_2,A_3) on the mean wetted surface of body *jb*, due to the motion of that body in the *j*-mode; *G(..)* is the Green's function or 'influence function" of a pulsating source located in (A_1,A_2,A_3) on the potential in a point located at (x,y,z) on body *ib*. The Green's function satisfies the equation of continuity, the linearized boundary condition on the free surface and on the sea floor and the radiation condition at infinity.

The unknown source strength function $\sigma_{ib,j}$ is determined based on the normal velocity boundary condition on the bodies:

$$\frac{\partial\phi_{ib,j}}{\partial n} = n_{ib,j} \cdot\cdot$$
$$\cdot\cdot = -\frac{1}{2}\sigma_{ib,j}(\vec{X}) + \sum_{jb=1}^{N_B}\frac{1}{4\pi}\iint_{S_{jb}}\sigma_{ib,j}(\vec{A}_{jb})\frac{\partial}{\partial n_{S_{jb}}}G(\vec{X},\vec{A}_{jb})dS_{jb} \qquad \text{(Eq. 9)}$$

with:

$n_{ib,j}$ = the direction cosine defined as follows:

$n_{ib,1} = \cos(n_{ib},x_{ib})$

$n_{ib,2} = \cos(n_{ib},y_{ib})$

$n_{ib,3} = \cos(n_{ib},z_{ib})$

$n_{ib,4} = y_{ib}n_{ib,3} - z_{ib}n_{ib,2}$

$n_{ib,5} = z_{ib}n_{ib,1} - x_{ib}n_{ib,3}$

$n_{ib,6} = x_{ib}n_{ib,2} - y_{ib}n_{ib,1}$

In (Eq. 9), the operator $^{\partial}/_{\partial n}$ signifies the gradient in the direction normal to the body surface. For the solution of the motion potentials, the right hand side of (Eq. 9) is given by the direction cosines. For the solution of the diffraction potential the right hand side is given by:

$$n_{ib,7} = \frac{\partial \phi_d}{\partial n} = -\frac{\partial \phi_0}{\partial n} \qquad \text{(Eq. 10)}$$

To solve (Eq. 9) numerically, the surface of each body is subdivided by $N_{p,ib}$ panels, which results in a set of equation with sum of $N_{p,ib}$ source strengths $\sigma_{j,ib,ip}$:

$$-\frac{1}{2}\sigma_{ib,ip,j} + \sum_{jb=1}^{N_B}\frac{1}{4\pi}\sum_{jp=1}^{N_{p,jb}}\sigma_{jp,jp,j}\frac{\partial}{\partial n}G_{ib,ip,jb,jp}\Delta S_{jp} = n_{ib,ip,j} \qquad \text{(Eq. 11)}$$
$$ib = 1,B;\ ip = 1,N_{p,ib};\ ip \neq jp$$

Domain Splitting

As example, Figure 2 is showing a two domain problem, where domain I is the outer domain and domain II is the gap domain; the dotted line is representing the boundary between the domains. The boundary is denoted with L (left) for the surface side belonging to domain I and R (right) for surface side belonging to domain II. The body surface area adjoining the outer domain I are indicated by S_I, the body surface area adjoining the gap domain II are indicated by S_{II}. The boundary surface is indicated by D.

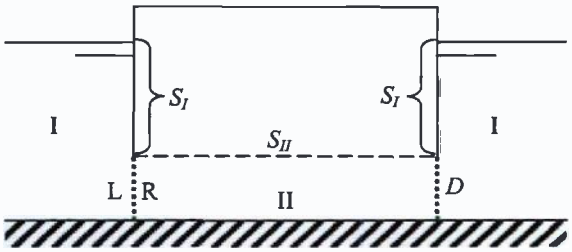

Figure 2: Domain boundary definition

Outer Domain

The outer domain is considered to be the part of the control volume where the standard 3D potential theory is applicable. The basic principles described above apply at this domain, with the additional boundary conditions at the boundary of other domains. As such, in the outer domain the following applies:

$$\phi_{outer} = \phi_0 + \frac{1}{4\pi}\iint_{S_I+D}\sigma_I G dS \qquad \text{(Eq. 12)}$$

Where S_I is representing the surface of all bodies and/or body parts which adjoin the outer domain and D is the surface describing the boundaries between domains.

Gap Domain

The gap domain is described by a 2-dimensional contour; this contour describes the boundary between the gap domain and other domains. More than one domain may be surrounding the gap domain; for example the outer domain and the submerged deck domain, as illustrated in Figure 3. The picture shows a red transparent cargo above an orange HTV, with a blue colored gap domain and two green colored submerged deck domains, the outer domain is indicated by the grey still water surface.

The basis for the gap domain is the assumption that a 2D-potential theory solution can be used. In addition, the wave potential does not have a direct influence on the inner domain; the influence of the wave is applied through the domain boundary (D). As a result the following applies:

$$\phi_{gap} = \frac{1}{4\pi}\iint_{S_{II}+D}\sigma_{II}G_2 dS \qquad \text{(Eq. 13)}$$

Investigations by Jonge [3] and Drobyshevsky [4] have shown that – for small gap height and small relative amplitude motions – this assumption is valid. However, as shown by Jonge and further illustrated in this paper large relative amplitude motions show highly non-linear behavior.

Submerged Deck + Dock Domain

For the submerged deck domain, the suitability to apply potential theory largely depends on the water level above the submerged deck. Ananthakrishnan [8] investigated submerged

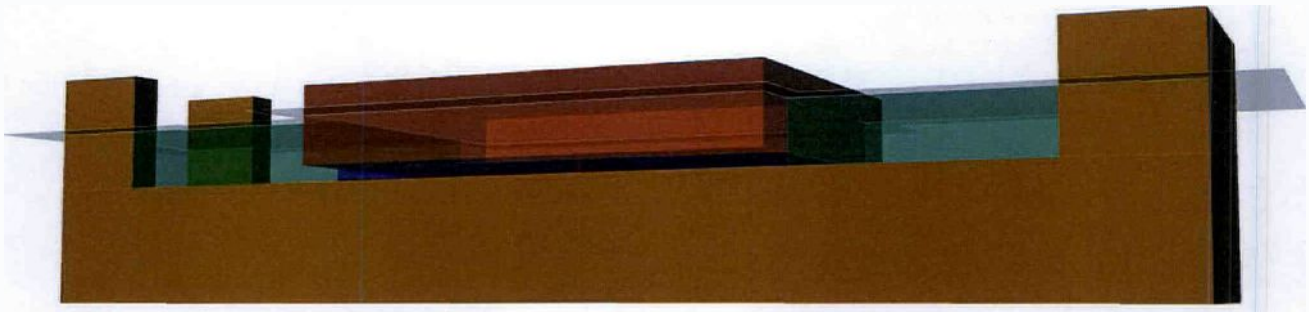

Figure 3: Example domain definition for cargo above HTV

cylinders using a viscous-flow formulation; it was clearly shown that at low and intermediate frequencies viscosity has significant effect on hydrodynamic forces. Also other researchers, like Ogilvie [9] and Chung [10], extensively investigated submerged objects. A more relevant paper was written by Newman [11]; which describes a matching method for a multi-domain problem of a submerged rectangular shape.

Similar assumptions can be made as for the submerged deck domain. Here, all expect one side of the domain is bound by the submerged body. It is assumed that inside the dock potential Φ_w – and thus Φ_d – is zero, at the dock opening the domain boundary condition applies.

Domain Boundary Condition

At the domain boundary, the normal velocity and the pressure on both sides need to be equal. The normal velocity condition is defined by (Eq. 14), in which the minus sign appears because of the opposite normal direction of the left-hand panels in domain I and the right-hand panels in domain II.

$$\frac{\partial \phi}{\partial n}_{left} = -\frac{\partial \phi}{\partial n}_{right} \qquad \text{(Eq. 14)}$$

The pressure condition follows from Bernoulli's equation, in which constant terms and velocity-squared terms are neglected in accordance with the linear theory:

$$\phi_L = \phi_R \qquad \text{(Eq. 15)}$$

Using discretization of the boundary surface, the normal velocity boundary condition on the domain boundary becomes:

$$\left\{\frac{1}{4\pi}\sum_{ib=1}^{N_{B,I}}\sum_{i=1}^{N_{P,ib}}\sigma_I(\vec{A}_{ib_i})\frac{\partial}{\partial n}G_I(\vec{X}_j^b,\vec{A}_{ib_i})\Delta S_{ib_i}\right\}_L + \left\{\frac{1}{4\pi}\sum_{jb=1}^{N_{B,II}}\sum_{i=1}^{N_{P,jb}}\sigma_{II}(\vec{A}_{jb_i})\frac{\partial}{\partial n}G_{II}(\vec{X}_j^b,\vec{A}_{jb_i})\Delta S_{jb_i}\right\}_R = v_{n_j}^{I-II} \qquad \text{(Eq. 16)}$$

with:

$v_{n_j}^{I-II}$ = the normal velocity j on boundary between domain I and domain II

$\vec{X}_j^b = (x, y, z)$, position vector of boundary field point j

$\vec{A}_{jb_i} = (A_1, A_2, A_3)$, position vector i of source on body jb

The expression within brackets denoted with index L or R refers to the influence of all sources on all bodies of domain I or II respectively on the normal velocity on the boundary panels on the left- or right-hand-side of the boundary.

In (Eq. 16) the influence functions G_I and/or G_{II} depend on the chosen solution in the domain I and II; for example inside a gap domain a 2D flow solution is used. The value of the right-hand-side of (Eq. 16) depends on the kind of domains I and II, for example if domain I is the outer domain and domain II is the gap domain then (Eq. 12), (Eq. 13) and (Eq. 14) results in:

$$v_{n_j}^{I-II} = \frac{\partial \phi_w}{\partial n} \qquad \text{(Eq. 17)}$$

Finally, to be able to solve the unknown source strengths, the set of equations for the boundary condition of equal pressure on the boundary surface is needed. Similar to (Eq. 14) and (Eq. 16), (Eq. 15) leads to:

$$\left\{\frac{1}{4\pi}\sum_{ib=1}^{N_{B,I}}\sum_{i=1}^{N_{P,ib}}\sigma_I(\vec{A}_{ib_i})G_I(\vec{X}_j^b,\vec{A}_{ib_i})\Delta S_{ib_i}\right\}_L - \left\{\frac{1}{4\pi}\sum_{jb=1}^{N_{B,II}}\sum_{i=1}^{N_{P,jb}}\sigma_{II}(\vec{A}_{jb_i})G_{II}(\vec{X}_j^b,\vec{A}_{jb_i})\Delta S_{jb_i}\right\}_R = \phi_{n_j}^{I-II} \qquad \text{(Eq. 18)}$$

And similar to (Eq. 17), combining (Eq. 12), (Eq. 13) and (Eq. 15), the right-hand-side of (Eq. 18) becomes:

$$\phi_{n_j}^{I-II} = \phi_w \qquad \text{(Eq. 19)}$$

By combining above equations, it is possible to solve the unknown source strengths. Next, the fluid pressures on each body, wave elevations, forces, added mass and damping can be determined following the usual way. Here, only panels representing the bodies need to be taking into account; domain boundary panels need not to be taking into account. Finally, equations of motions can be solved, possibly accounting coupling in terms of stiffness due to cargo handling equipment between bodies.

Validity

The above solution ensures that the velocity potential and pressures are matched between the domains, whereas the method used by Jonge [3] did not yet do this. Instead, Jonge first solved the velocity potential in the gap domain and next solved the velocity potential and pressures in the outer domain; thus the solution between domains were not fully "matched".

However, the above proposed is only valid under the assumption that linearization is possible; higher order terms and quadratic terms are neglected. For Offshore Loading and Discharge, this may be valid to some extend as operational sea conditions are generally low. On the other hand, as shown below by model testing, for the gap domain this may not be true.

Further investigation of theory and model tests is required; if possible changes to above proposed solution is needed and/or empirical methods may have to be found. Depending on findings it may not be possible to solve the Offshore Loading and Discharge problem solely based on frequency domain analysis. Instead combining the linearized characteristics – found with above solution – with empirical or other solutions in a time-domain approach may be required.

MODEL TESTS AT SHALLOW WATER

As research is ongoing, the above theory is not yet implemented in a multi-body multi-domain code. First, more insight in the gap problem is obtained by performing model tests. With more insight, it may be possible better distinguish linear and non linear effects. Future work is to further

investigate the theory and/or find ways to account for the non-linear effects; either by further adapting above described theory or coupling above theory to other methods (e.g. CFD or VoF).

In 2008 a short test series was performed to explore the effects of narrow gap flow. At that time a limited set of tests with a cylindrical shape was done; variations consisted of three frequencies, three amplitudes of vertical motion and two gap heights. In 2010, this test series was extended with more frequencies and with the other basic shapes mentioned above. Also rotational oscillation tests were performed; these are not presented in this paper.

To investigate the gap domain contour, four basic shapes were tested. The shapes are representative for cargos often transported. Pictures of the four models – cylinder, triangle, square and ring – are shown in Annex B. The bottom area of the cylinder, triangle and square were kept equal; the moon pool area of the ring is a quarter of the area of the square.

An important difference between the test done in 2008 and 2010 is the test basin; in 2010 the tests were carried out in a narrow towing tank, which causes wall-effects to influence the measurements; this became evident from observed standing wave pattern during several tests. The tests in 2008 were performed in a large shallow water basin. This difference is not a problem, as long as calculations are also performed with the walls. Also, the walls are comparable to the bulkheads of HTVs, especially similarity is seen for type-2 vessels.

Measurement results and observations

In Annex C, measurement results of the model tests are shown for the different shapes. Figure 14 shows the mean value and standard deviation of the measured vertical force; Figure 15 shows the maximum and minimum amplitude. These figures show that the triangle, cylinder and square exhibit similar trends of mean, standard deviation and amplitudes; the ring shape shows a different trend. The circular markers indicate repeated test; it is evident that the mean values are – as they are small – not reproduced accurately, while standard deviation and amplitudes are.

Figure 4 is showing force measurement for the cylinder at different amplitudes; forces are divided by the maximum motion amplitude and the motion signal is made dimensionless. For large amplitudes large troughs are shown, which become larger with increasing motion amplitude; the troughs start when the motion is turning upward. Apparently, a large force is needed to suck water back into the gap. This phenomenon can be compared to what in practice is known as a sticking effect during cargo float-off, where it can take a short while before cargo is coming of the cribbing when a HTV is submerging. Based on Figure 4, it is concluded that there is a force component linear dependent on motion amplitude and a non-linear force component identified as suction force phenomenon. As may be expected the phase between motion and force does not change with amplitude.

In Figure 5 and Figure 6, the force measurement for the different shapes is compared; two typical cases are shown. Comparison of the different shapes shows that the shape of the model has marginal influence on the measured force; influence is mainly seen in the suction force troughs occurring at high frequencies. For low frequencies a shift in mean values and a small difference in amplitude are observed; higher order fluctuation is seen on all cases and seems to show similar trends. Visual observation of the test showed large regions of turbulent flow, together with the higher order fluctuations seen in the force signals; there are signs of vortices shedding of the sharp edges of the models. In case of the ring shape, the results are strongly influenced by the moon pool; visual observation showed large vertical oscillation of the water surface inside the moon pool. The suction force phenomenon is less pronounced.

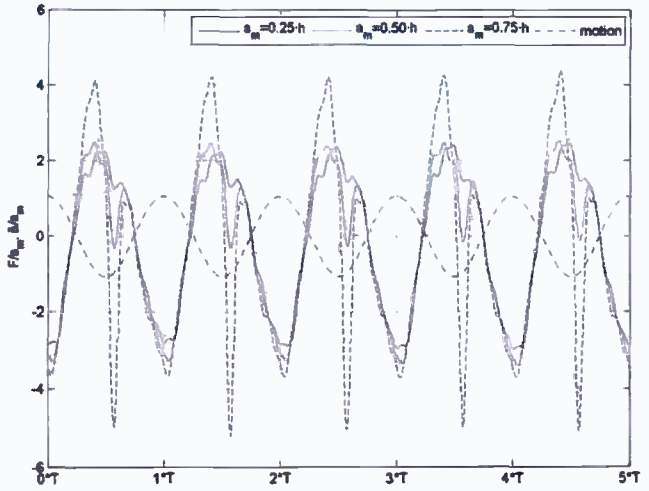

Figure 4: Cylinder, d/h=20, f=0.338 Hz

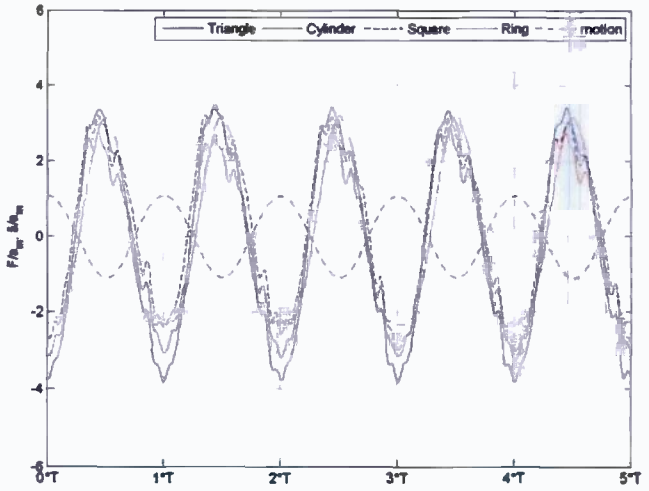

Figure 5: Comparison Shapes – a_m=0.25·h, d/h=40, f=0.281 Hz

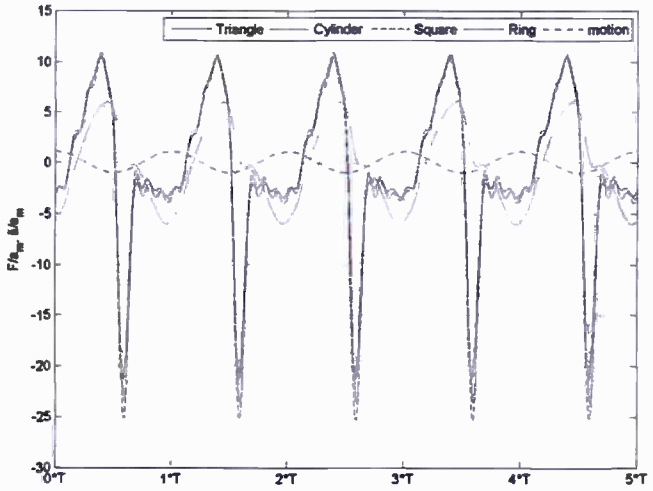

Figure 6: Comparison Shapes – a_m=0.75·h, d/h=40, f=0.450 Hz

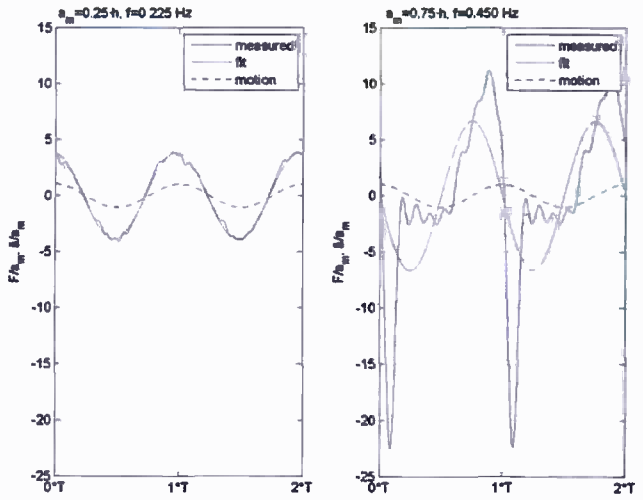

Figure 7: Curve fitting

Model test processing

By fitting a sinusoidal signal on the measured force by a least square method, it is possible to estimate the added mass and damping. Based on rewriting the basic equation of motion and separating the in-phase and out-phase components, the added mass and damping are determined using the equations:

$$A_{33} = \frac{-C_{33} \cdot z + F\cos(\varepsilon)}{-\omega^2 \cdot z} - M \qquad \text{(Eq. 20)}$$

$$B_{33} = \frac{F\sin(\varepsilon)}{\omega \cdot z} \qquad \text{(Eq. 21)}$$

In Figure 7 a typical example of the time-series is shown in which the best fit of sinusoidal signal on the measured force is added. An example of resulting added mass and damping based on this fitting is shown in Figure 8. It is evident that this fitting may not be appropriate for all tests. Generally, for low frequencies and low motion amplitudes, the fit is valid. For high frequencies and high amplitudes the suction force troughs are strongly influencing the fit; the fitted curve seems to shift and thus phase angle between motion and force is changing. It is evident from (Eq. 20) and (Eq. 21) that this has an impact on ratio between added mass and damping; this is supported by the comparison made in Figure 4, where phase between motion and force seems not to be changing depending on amplitude.

Figure 8 is also showing a comparison between the test carried out in 2008 and 2010. As mentioned an important difference was the test facility; apparently the tank walls are effecting the measurements significantly.

Generally, it is seen that the added mass and damping for the different shapes – except the ring – are very similar; and of course dependent on the gap height. This is shown in Figure 9. Only the measurement for the triangle at f=.281 Hz and d/h=40 seems to deviate from the trend; this may be caused by measurement error, wall effect, inaccuracy in processing or physical phenomenon. Further analysis is required.

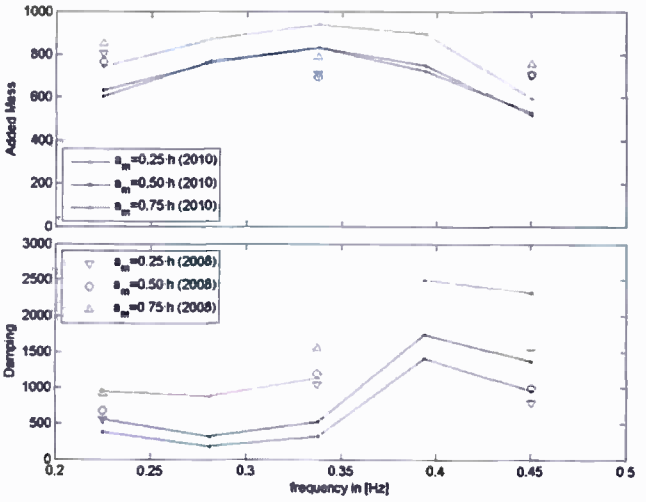

Figure 8: Added mass and damping – Cylinder

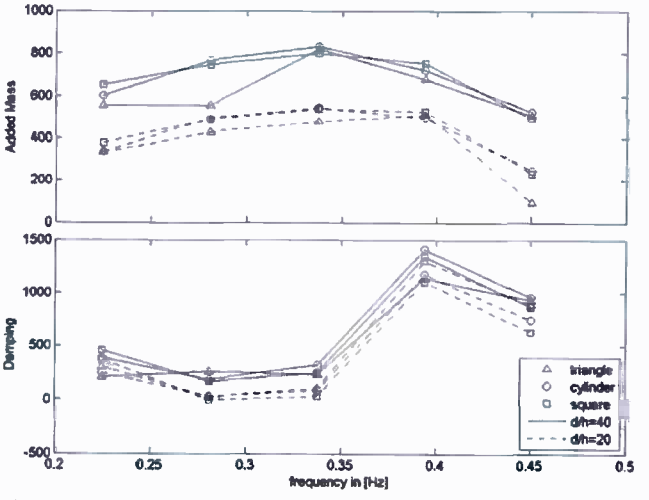

Figure 9: Added mass and damping – a_m=0.25·h

CONCLUSIONS

For the assessment of hydrodynamic behavior of HTV and cargo during offshore loading and discharge, a linear potential theory is presented, which can cover problems with multiple complex bodies and fluid domains. By specifying different domains – in which different potential solutions may be used – with specific boundary conditions dependent on the nature of each domain, it is possible to find the linearized hydrodynamic characteristics. The past has shown that such similar methods give reasonable accurate linear results.

By performing oscillation tests, more insight in the phenomenon related to the narrow gap flow is gathered; large suction forces non-linear dependent on the motion amplitude are observed. Further the measured forces are weakly dependent on the model shape. For the tested ring shape, the gap influence is small, while the moon pool has a strong influence; standing wave elevation inside the moon pool is very large.

It is concluded from the tests that the forces may be split in a linear and a non-linear component. It is expected that the linear part will be predicted accurately by above presented theory. Further investigation is required to find a method for predicting the non-linear component.

FUTURE WORK

The research project will consist of further investigating the phenomenon related to the gap flow; separation of linear and non-linear force components is needed to find appropriate methods to predict both. The above mentioned multi-domain diffraction method will be implemented in computer code – where possible improved. Above test cases and results will be analyzed using this code; results may assist in investigating the force components.

Tests with a submerged HTV alone and with cargo floating above are envisaged; these tests are needed to further verify motion prediction and to gather insight and data of loads for handling cargo during discharge and offloading operations. With this knowledge, methods can be further improved where necessary. System concepts may be design for cargo handling equipment. Finally, analysis and design for offshore loading and discharge can be carried out, reflecting – amongst others – design operational condition, operability/downtime, system designs and operational procedures.

NOMENCLATURE

CFD	= Computational Fluid Dynamics
HTV	= Heavy Transport Vessel
MDDM	= Multi Domain Diffraction Method
TLP	= Tension Leg Platform
VoF	= Volume of Fluid method
$\tilde{a}$	= amplitude in time
a_m	= maximum amplitude
A_{33}	= Added mass for heave motion
B_{33}	= Damping for heave motion
C_{33}	= Stiffness for heave motion
d	= equivalent diameter
f	= frequency
F	= force
h	= gap height
M	= model mass
$\vec{n}_{ib}$	= normal vector of body *ib*, positive into the fluid
S_{ib}	= mean wetted surface of body *ib*
$\vec{v}_{ib}$	= velocity vector of a point on body *ib*
z	= heave motion amplitude
ε	= phase angle between force and motion
ω	= wave frequency

ACKNOWLEDGMENTS

This research is made possible by DOCKWISE; time and money is seen as an important investment for the company and employees involved, which is very much appreciated by the author. The author also highly appreciates the assistance from Delft University of Technology.

REFERENCES

[1] STRATEN, O. VAN, Thesis Report No 1207-S, Delft University of Technology, 1999

[2] BASS, D., et. al., 'Simulating Wave Action in the Well Deck of Landing Platform Dock Ships using Computational Fluid Dynamics', Warship 2004

[3] JONGE, J. DE, et. al., 'A Hydrodynamic Analysis Method for Offshore Discharge Operations', OMAE2008-57155

[4] DROBYSHEVSKI, Y., 'An Efficient Method for Hydrodynamic Analyses of a Floating Vertical Sided Structure in Shallow Water', OMAE2006-92118

[5] PINKSTER, J., 'Suction, Seiche and Wash Effects of Passing Ships in Ports', 024.R3, SNAME Annual meeting conference, Providence, Rhode Island, 2009

[6] IKOMA, T., et. al., 'Prediction Methods for a Hydroelastic Behavior of an Aircushion Supported Elastic Floating Structure', Pacific Congress on Marine Science and Technology, 2002

[7] TUCK, E.O., 'Matching Problems Involving Flow through Small Holes', Advances in Applied Mechanics 15, 89-158. 1975

[8] ANANTHAKRISHNAN, P., 'Heave Oscillations of a Submerged Vertical Cylinder in a Viscous Fluid', IJOPE, Vol. 8, No. 3, pp. 173-181, Sept. 1998

[9] OGILVIE, T.F., 'First- and Second Order Forces on a Cylinder Submerged under a Free Surface', Journal of Fluid Mechanics, Vol. 16, No.3, 1963

[10] CHUNG, J.S., 'Forces on Submerged Cylinders Oscillating near a Free Surface', J. of Hydrodynamics, Vol.11, No.3, 1977

[11] NEWMAN, J.N., et. al., 'Added Mass and Damping of Rectangular Bodies Close to the Free Surface', J. of Ship Research, Vol.28, No.4, 1984

ANNEX A

HEAVE TRANSPORT VESSELS

Figure 10: Type-0 – Open stern+bow HTV

Figure 11: Type-1 – Open Stern HTV

Figure 12: Type-2 – Closed Stern HTV

Figure 13: Type-3 – Dock-type HTV

Table 1: HTV types

		Type	Company	Deadweight
1	Type-0 (2012)	Open-stern	Dockwise	115,000
2	Blue Marlin	Open-stern	Dockwise	76,292
3	Black Marlin	Open-stern	Dockwise	57,021
4	Mighty Servant 1	Open-stern	Dockwise	40,910
5	Mighty Servant 3	Open-stern	Dockwise	27,720
6	Transshelf	Open-stern	Dockwise	33,700
7	Super Servant 3	Open-stern	Dockwise	14,138
8	Super Servant 4	Open-stern	Dockwise	14,059
9	Fjord	Open-stern	Fairstar	24,500
10	Fjell	Open-stern	Fairstar	19,300
11 - 12	FORTE (2012) + FINESSE (2012)	Open-stern	Fairstar	50,000
13	Tai An Kou	Open-stern	NMA/COSCO	20,131
14	Kang Sheng Kou	Open-stern	NMA/COSCO	18,000
15 - 16	Xiang Yun Kou (2010) + Xiang An Kou (2011)	Open-stern	NMA/COSCO	50,000
17	Mega Passion	Open-stern	MegaLine	63,000
18	Wish Way	Open-stern	CCCC	20,000
19	STX Rose	Open-stern	STX Pan Ocean	16,715
20	Mighty Dragon (2012)	Open-stern	COOEC	50,000
21	Hua Tian Long (2011)	Open-stern	Guangzhou Salvage	30,000
22 - 25	2 new (>2012) + 2 optional	Open-stern	United Faith	50,000
26	design phase	Open-stern	United Faith	80,000
27 - 32	6 x T-class	Closed-stern	Dockwise	53,868
33 - 34	Swan + Tern	Closed-stern	Dockwise	32,650
35 - 36	Swift + Teal	Closed-stern	Dockwise	32,187
37 - 38	Eagle + Falcon	Closed-stern	OHT	31,809
39 - 40	Osprey + Hawk	Closed-stern	OHT	54,000
41	Development Way	Closed-stern	CCCC	25,000
42	Yacht Express	Dock-type	Dockwise	9,400
43	Explorer	Dock-type	Dockwise	10,763
44 - 45	Rolldock Sun + Sea	Dock-type	Rolldock	8,300
46 - 47	Rolldock Sky (2011) + Star (2012)	Dock-type	Rolldock	8,300
48 - 51	4 x Rolldock (2012-2013)	Dock-type	Rolldock	8,300
52 - 56	CONDOCK I-V	Dock-type	Condock	3,603-4,500
57 - 60	Combi Dock I-IV	Dock-type	CombiLift	11,000

ANNEX B

MODEL TESTS SET-UP

ANNEX C

MODEL TESTS RESULTS

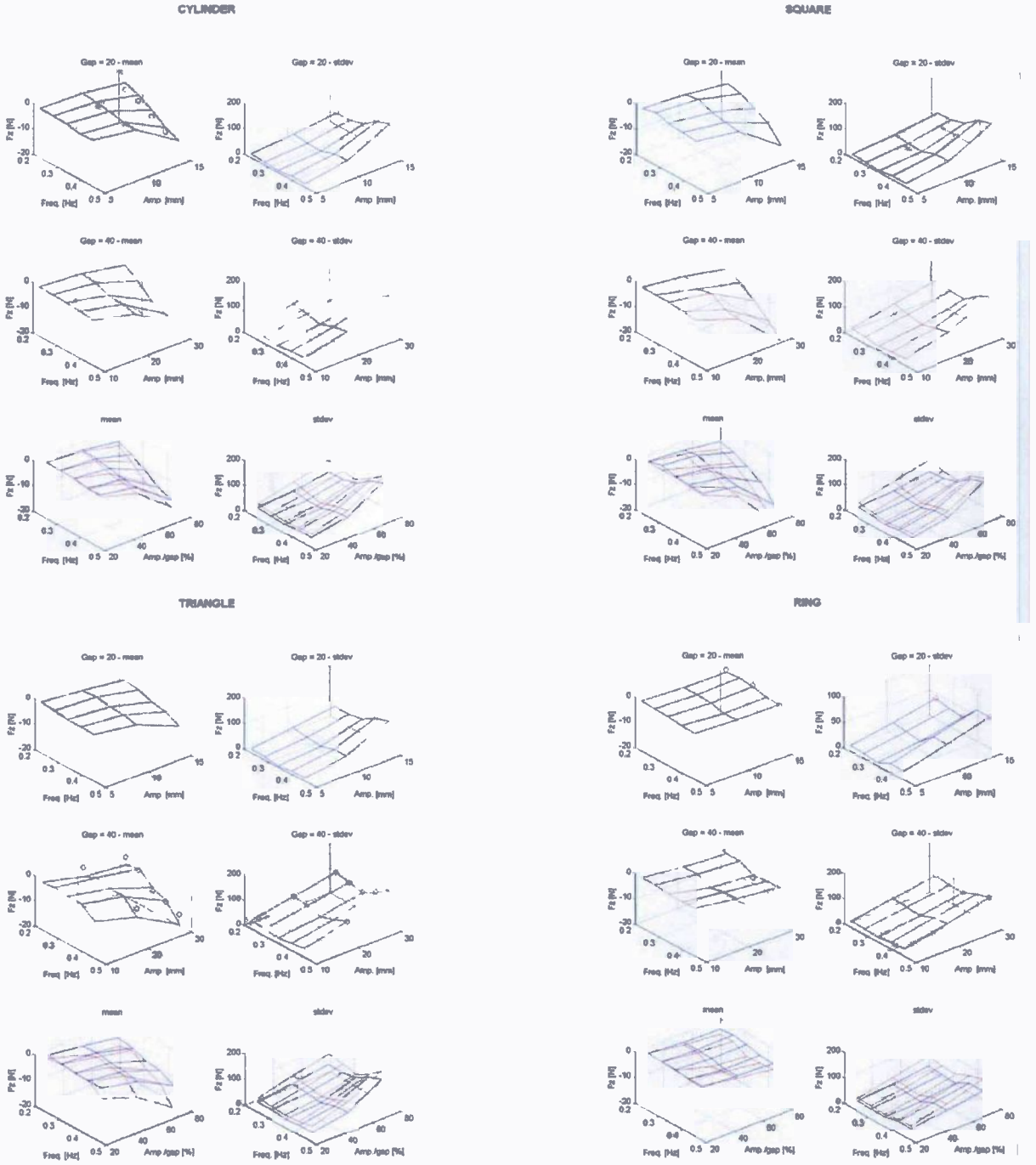

Figure 14: Model test measurement – mean and standard deviation

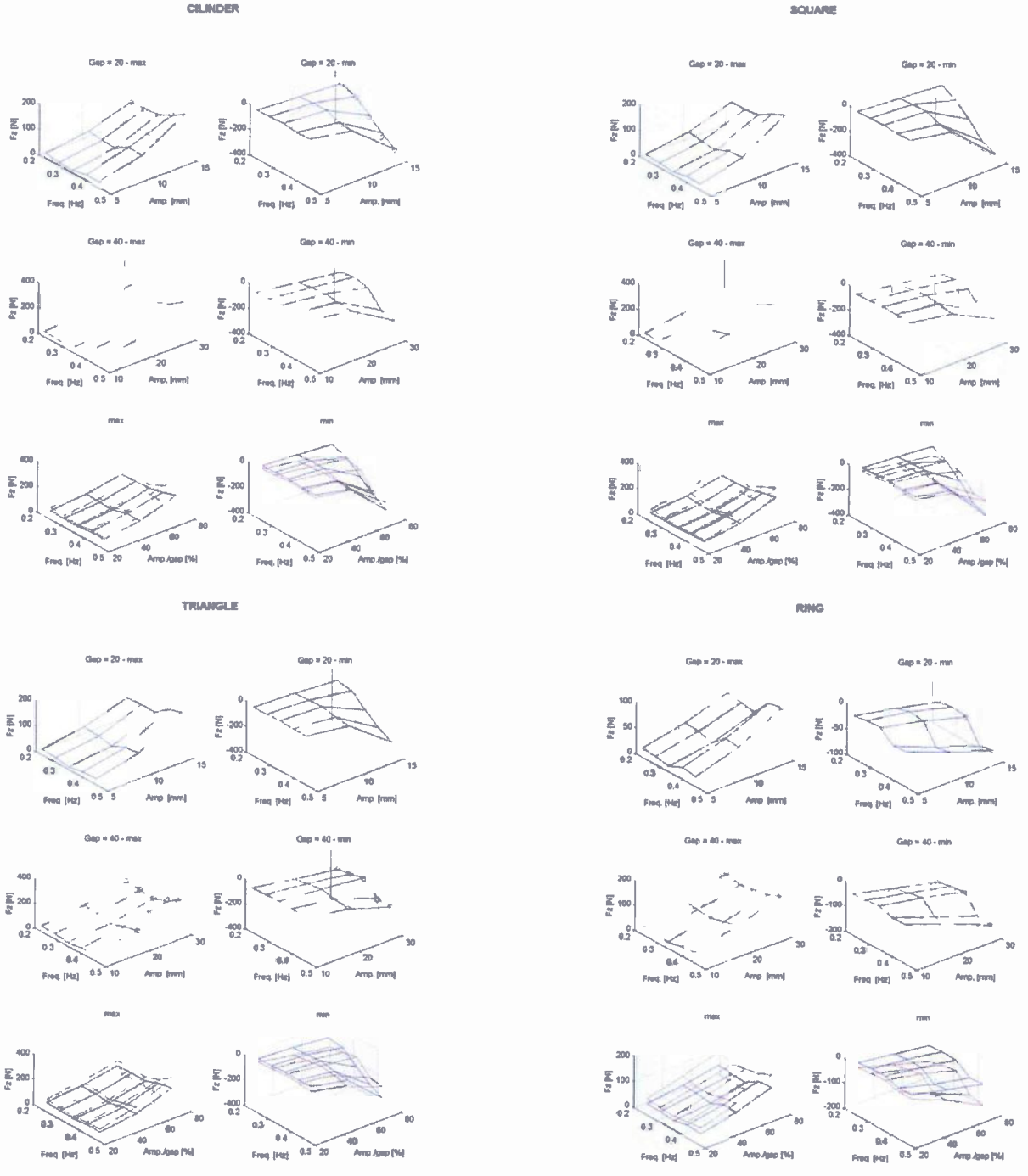

Figure 15: Model test measurement – maximum and minimum